Available Online

JOURNAL OF SCIENTIFIC RESEARCH

J. Sci. Res. **17** (1), 133-140 (2025) www.banglajol.info/index.php/JSR

Estimating Coalescence Time in Disdrometer Drop Size Distributions: A PYSDM Cloud Modeling Approach

N. H. Shah[1], J. Chahal[2*], B. P. Shukla[3], A. Priamvada[2]

[1]Department of Mathematics and School of Emerging Science & Technology, Gujarat University, Ahmedabad-380009, India

[2]Department of Mathematics, Gujarat University, Ahmedabad-380009, India

[3]Environment Sciences Division, Space Applications Centre, ISRO, Ahmedabad-380015 Gujarat, India

Received 23 June 2024, accepted in final revised form 21 October 2024

Abstract

Cloud droplet evolution is influenced by microphysical processes such as nucleation, condensation, evaporation, and coalescence, all of which impact precipitation. Models simulating droplet growth help improve rainfall predictions by providing insight into these processes. In this study, we investigate the coalescence time of droplets, using ground truth data from Disdrometer Observations with a size range of 156.5 to 2800.25 µm, applying the Python Super Droplet Model (PySDM) to simulate the evolution of droplet size over time. Focusing on the coalescence process, we analyzed the time-dependent progression of droplet formation. Our results revealed a relationship between coalescence time (CT) and drop size distribution (DSD). Larger droplets were found to coalesce rapidly upon impact, quickly reaching a precipitation-ready state, while smaller droplets experienced more frequent bouncing, requiring more time for coalescence. The mean coalescence time was estimated to be approximately 12,550 sec.

Keywords: Super droplet method; Disdrometer; Cloud microphysics; Monte-Carlo simulation; Coalescence.

doi: https://dx.doi.org/10.3329/jsr.v17i1.74290 J. Sci. Res. **17** (1), 133-140 (2025)

1. Introduction

Rainfall results from intricate interactions between microphysical and dynamical processes in the earth-atmosphere system, with factors such as raindrop size distribution (DSD), atmospheric pollutants, and long-term climatic trends playing critical roles. DSD is integral to understanding rainfall mechanisms, impacting agriculture, ecosystems, and public health. For instance, pollutants like PM2.5, PM10, and black carbon (BC) in Bengaluru alter cloud microphysics, affecting droplet formation and precipitation [1]. Similarly, atmospheric conditions influenced by geomorphic features affect groundwater recharge, with pediplains

* *Corresponding author*: jyotichahall.jc@gmail.com

offering higher yields [2]. The Atmospheric Boundary Layer (ABL) height, which influences pollutant dispersion through the Ventilation Coefficient (VC), is significantly affected by fog, as observed in Delhi [3]. Long-term climatic trends further complicate this picture. An increasing trend in rainfall has been observed in Ranchi, with a negative correlation between rainfall and temperature in several months [4]. This is supported by the use of ARIMA models to forecast rising rainfall trends in Chattogram, Bangladesh, particularly during the monsoon season [5]. DSD's impact on rainfall is further explored through studies on soil erosion and radar hydrology. DSD affects soil erosion and rainfall kinetic power [6], while radar reflectivity and rain rate relationships through DSD have been examined [7]. The negative exponential distribution of DSD given by equation 1 is crucial for understanding these dynamics [8].

$$N(D) = N_0 exp(\Lambda D)\ (0 \le D \le D_{max}) \quad (1)$$

where $N_0(m^{-3}cm^{-1})$ and $\Lambda\ (cm^{-1})$ are the distribution parameters, D_{max} is the maximum diameter of the raindrops [9]. The evolution of cloud droplets, influenced by processes such as nucleation, condensation, and coalescence, is essential for accurate rainfall predictions. Smoluchowski's coagulation equation (SCE) in 2, described by Norris [10] and evaluated by Hocking and Jonas [11], balances cloud particle populations

$$\frac{\partial n(x,t)}{\partial t} = \frac{1}{2}\int_0^x K(x-y,y)\ n(x-y,t)\ n(y,t)dy - \int_0^\infty K(x,y)\ n(x,t)\ n(y,t)dy \quad (2)$$

where $n\ (x,t)$ is the number density of particles as they coagulate to size x at time t and $K(x,y)$ is the coagulation kernel. Moore [12] linked droplet size with atmospheric pollutants, and Liou [13] examined the relationship between liquid water content and precipitation. Telford [14] introduced the stochastic coalescence model (SCM), further analyzed by Gillespie [15], while Gebauer [16] explored how DSD influences coalescence. The Python-based super droplet model (PySDM), leveraging super droplet methods and Monte-Carlo algorithms, provides valuable insights into aerosol-cloud interactions and cloud microphysics [17,18]. This study focuses on the impact of coalescence on the temporal evolution of cloud droplets, utilizing PySDM and RD-80 Disdrometer data.

2. Data Used (RD-80 Disdrometer)

This study leverages RD-80 Disdrometer data to investigate rainfall microphysics by integrating it with the PySDM model, which is designed to elucidate cloud microphysical processes. Using the high-accuracy data from the Disdrometer, we analyze coalescence dynamics and their impact on rainfall. The Disdrometer provides precise measurements of various rainfall parameters, including droplet number density within radius bins (156.5 to 2800.25 μm) shown in Table 1, rainfall intensity, rate, radar reflectivity, and kinetic energy, all recorded every 30 seconds. These measurements are based on the electrical impulses generated by raindrops impacting the sensor, which are inversely related to drop diameter, as detailed by Bartholomew [19].

Table 1. Radius bins for RD-80 Disdrometer [19].

Classes	Radius bins (μm)	Classes	Radius bins (μm)
Class 1	156.5-202.5	Class 11	874.0-1038.5
Class 2	202.5-252.5	Class 12	1038.5-1205.0
Class 3	252.5-298.0	Class 13	1220.5-1363.5
Class 4	298.0-357.5	Class 14	1363.5-1505.5
Class 5	357.5-413.5	Class 15	1505.5-1692.5
Class 6	413.5-499.5	Class 16	1692.5-1852.0
Class 7	499.5-616.0	Class 17	1852.0-2063.5
Class 8	616.0-714.5	Class 18	2063.5-2286.5
Class 9	714.5-791.0	Class 19	2286.5-2572.5
Class 10	791.0-874.0	Class 20	2572.5-2800.25

3. Methodology

This study focuses on the 'Coalescence' phenomenon using the Super Droplet Model (PySDM), with RD-80 Disdrometer data serving as ground truth. We compare observed raindrop number density from the Disdrometer with the PySDM mass density by converting observed number density into mass density using the formula:

$$\text{Mass density } (kg/m^3) = \frac{(Number\ Density \times Molar\ mass\ H_2O)}{Avogadro\ constant},$$

Where, Molar mass of H_2O is 18.015 g/mol, and Avogadro constant is 6.022×10^{23} particles/mol. We measured the onset and end of coalescence by running the model for up to 20,000 seconds, noting changes in mass density to determine coalescence start (Starting CT), end (Ending CT), and total duration (Total CT). An empirical rule is applied to predict coalescence duration for Disdrometer radius bins. This integration of PySDM and Disdrometer data bridges atmospheric dynamics with surface observations. The Super Droplet Model (SDM) differs from traditional methods by working with clusters of droplets, or 'super droplets,' each representing multiple droplets with identical properties.

4. Super Droplet Method (SDM)

The Super Droplet Model (SDM) uses clusters of droplets, or 'super droplets,' unlike traditional methods that focus on individual droplets. Each super droplet contains multiple droplets with the same attributes and evolves dynamically due to coalescence phenomena. The pattern of the coalescence of super droplets described below

In the coalescence of (i, j) pair of super droplets with the multiplicity ξ_i and ξ_j respectively the below cases show the updated variables $(x_i^{'}, R_i^{'}, M_i^{'})$ after the collision under SDM [17,18], where (x_i, R_i, M_i) are the position, equivalent radius of water, and solute mass of the super droplet.

1) When the number of droplets within the super droplets undergoing coalescence differs i.e. $\xi_i \neq \xi_j$, assume $\xi_i > \xi_j$ then the updated variables are:

$\xi_i' = \xi_i - \xi_j$, $\xi_j' = \xi_j$; $R_i' = R_i^{org}$, $R_j' = (R_i^3 + R_j^3)^{1/3}$; $M_i' = M_i^{org}$, $M_j' = (M_i^{org} + M_j^{org})$; $x_i' = x_i^{org}$, $x_j' = x_j^{org}$

2) When the number of droplets within the super droplets undergoing coalescence is same i.e. $\xi_i = \xi_j$ then, updated variables are:
$\xi_i' = [\xi_i/2],\ \xi_j' = \xi_i - [\xi_i/2],\ R_i' = R_j' = (R_i^3 + R_j^3)^{1/3},\ M_i' = M_j' = (M_i^{org} + M_j^{org}),\ x_i' = x_i^{org}\ \ , x_j' = x_j^{org}$

As time progresses, the variables evolve as a result of the coalescence of super droplets. Using these updated variables, we derive the distribution of mass density of droplets through an equation.

$$g(\ln R) = \frac{1}{\Delta V}\sum_{i=1}^{N_s}\xi_i m_i W_\sigma(\ln R - \ln R_i), W_\sigma(Y) = \frac{1}{\sqrt{2\pi}\sigma}\exp(-Y^2/2\sigma^2)\cdot \tag{3}$$

Where $\Delta V = 10^6 m^3$ is the volume of coalescence cell, $\sigma = \sigma_0 N_s^{\frac{-1}{5}}$ ($\sigma_0 = 0.62$) and $N_s = 2^{15}$ is the number of super droplet.

5. Empirical Rule on Standard Deviation

The empirical rule in equation 4 provides approximations for the proportion of data that falls within certain intervals around the mean in a normal distribution [20].

$$P(a \le X \le b) = \frac{1}{\sqrt{2\pi}\sigma}\int_a^b \exp(-\frac{1}{2}(\frac{x-\mu}{\sigma})^2)\ dx \tag{4}$$

One standard deviation is $P(\mu-\sigma \le X \le \mu+\sigma) \approx 0.68$, where μ is the mean and σ is the standard deviation, Second Standard Deviation is $P(\mu-2\sigma \le X \le \mu+2\sigma) \approx 0.95$ and Third Standard Deviation is $P(\mu-3\sigma \le X \le \mu+3\sigma) \approx 0.99$, by which we can say that the 68 % of data lie between the first deviation about the mean, 95 % of data lies between the second standard deviation about a mean. And the third standard deviation about the mean covers 99 % of the data [21,22].

6. Results and Discussion

The evolution of droplets according to the super droplet theory, as previously discussed, is illustrated in Figs. 1(a) and 1(b).

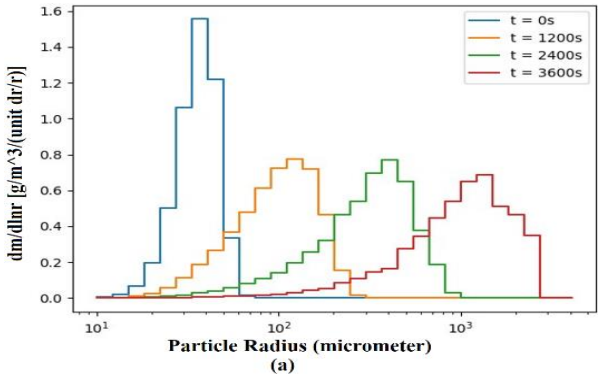

(a)

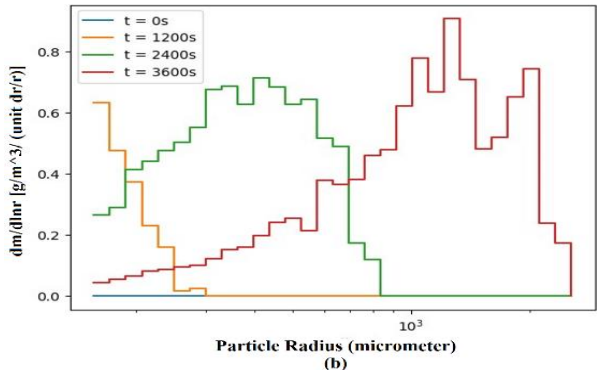

Fig. 1. Mass density distribution of super droplet at different time (a) for radius range between (10 µm-5000 µm) PySDM original radius bin done by Shima et.al. [11], (b) radius range between (156.5 µm -2800.25 µm) Disdrometer radius bin.

At the initial moment (t = 0) seconds, there is an absence of observed mass density within the Disdrometer radius bin shown in Fig. 1b. Conversely, in Fig. 1a, where the radius bins are of smaller scale compared to the Disdrometer radius bin, the presence of mass density is observed.

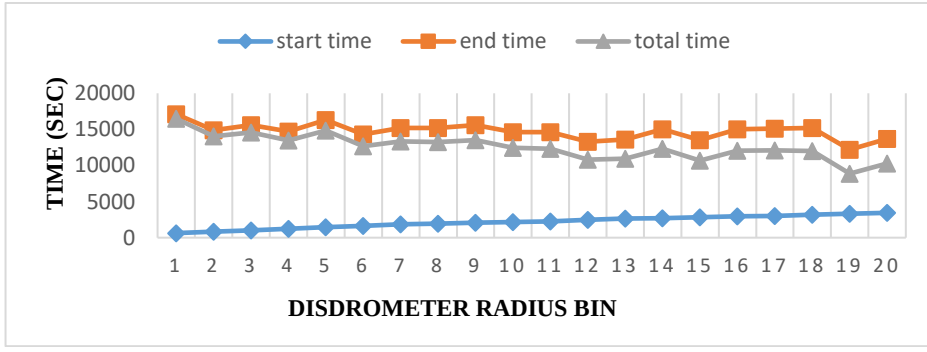

Fig. 2. The coalescence time of the super droplet determined by PySDM model for Disdrometer radius bin.

This suggests that the commencement of coalescence happens promptly for smaller droplets, while there's a delay in coalescence initiation for larger droplets which is also validated by [23-25]. This observation is further supported by the recorded time for droplet coalescence from the Disdrometer radius bin, as illustrated in Fig. 2 and analyzed using PySDM. Notably, the total coalescence time diminishes as droplet size increases.

In Fig. 2, it's evident that the duration of coalescence is influenced by both the onset and cessation times of coalescence for the droplets. The analysis determined a negative correlation between the total coalescence time for droplets and the time at which coalescence begins. This negative correlation is quantified by a correlation coefficient of -0.8702, as depicted in Fig. 3a.

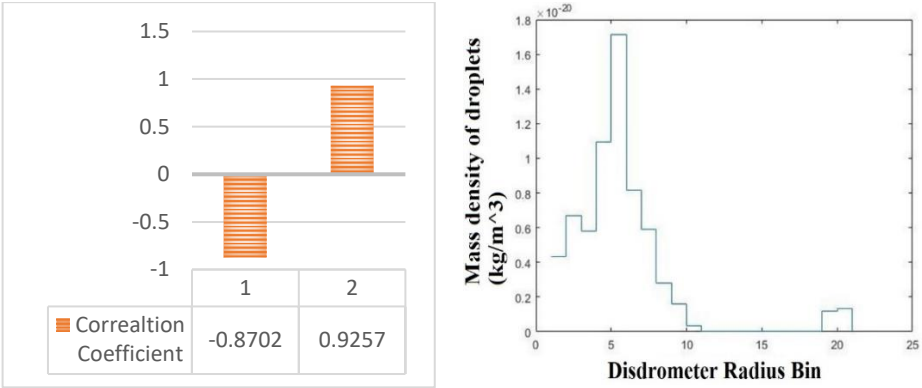

Fig. 3. (a) Correlation coefficient of total CT with the starting and ending time. (b) Mass density of droplets derived from the observed number density of rain droplets within each radius bin of the Disdrometer.

In Fig. 1a (plot by Shima), the mass density distribution is depicted following a normal distribution pattern. This characteristic is similarly observed in the mass density distribution within the Disdrometer radius bin analyzed through PySDM. To further affirm this observation, Cross-validation was performed using the actual ground truth data obtained from the Disdrometer, specifically examining the observed drop size distribution in terms of mass density at the 1200-sec mark (20 min), as illustrated in Fig. 3b. This confirms that super droplet theory is followed by the radius bins of Disdrometer data. Since the coalescence time for the droplets follows a normal distribution, the third standard deviation rule (Empirical rule) was applied to the total time of droplet coalescence to predict the duration of coalescence dynamics in any given environment., as illustrated in Fig. 4.

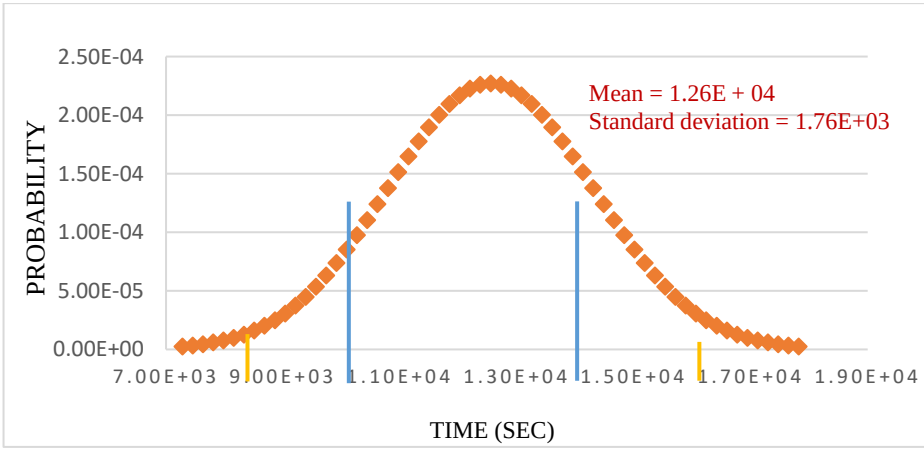

Fig. 4. Probability plot for Third standard deviation about mean.

Approximately 68 % of the total droplets complete the coalescence process within one standard deviation of the mean. this corresponds to a range of 10800 sec (180 min or 3 h) to 14300 sec (238 min or approximately 4 h), 95 % of the droplets in any environment complete the coalescence process within two standard deviations of the mean. This translates to a range of 9210 sec (153 min or 2.5 h) to 16100 sec (268 min or 4.5 h). And around 99 % of the data falls within three standard deviations of the mean. this means the coalescence process occurs between 7280 sec (121 min or 2 h) and 17800 sec (296 min or 5 h). These ranges provide estimates of the duration of the coalescence process for different percentages of droplets, giving insight into the variability and spread of the data.

7. Conclusion

The study concludes that the coalescence dynamics analyzed by PySDM and the observed number density of droplets provide consistent density distribution patterns. This suggests that PySDM effectively captures the behavior of droplet coalescence, aligning well with the observed data from the Disdrometer**.** Notably, the starting coalescence time is directly proportional to the droplet size distribution (DSD), implying that larger droplets take longer to initiate coalescence. Furthermore, it is discovered that the CT is normally distributed (a symmetric bell-shaped curve). By the sigma rule it can be inferred that 68 %, 95 %, and 99.7 % of the data have CT of 3-4 h, 2.5-4.5 h, and 2-5 h respectively. This will further help to improve precipitation modeling and forecasting, especially in tropical regions.

Acknowledgment

The authors express sincere gratitude to the Director of Space Applications Center (SAC), ISRO Ahmedabad, for his guidance and support. A part of the research was carried out under the ISRO-SMART Research Initiative Program. The authors thank anonymous reviewers for their constructive comments.

References

1. M. Shivkumar, T. S. Pranesha, K. R. Sudhindra, D. M. Chate, and G. Beig, J. Sci. Res. **15**, 335 (2023). https://doi.org/10.3329/jsr.v15i2.61403
2. Fuladi and M. S. Deshmukh, J. Sci. Res. **15**, 607 (2023). https://doi.org/10.3329/jsr.v15i3.63239
3. P. Singh, K. Soni, A. S. Nair, N. Kumar, and R. Sharma, J. Sci. Res. **14**, 813 (2022). https://doi.org/10.3329/jsr.v14i3.58317
4. C. K. Pandit, A. K. Lal, and U. S. Singh, J. Sci. Res. **16**, 723 (2024). https://doi.org/10.3329/jsr.v16i3.71668
5. M. H. Masum, R. Islam, M. A. Hossen, and A. A. Akhie, J. Sci. Res. **14**, 215 (2022). https://doi.org/10.3329/jsr.v14i1.54973
6. M. A. Serio, F. G. Carollo, and V. Ferro, J. Hydrol. **576**, 210 (2019). https://doi.org/10.1016/j.jhydrol.2019.06.040
7. R. Uijlenhoet, Hydrol. Earth Syst. Sci. **5**, 615 (2001). https://doi.org/10.5194/hess-5-615-2001
8. J. S. Marshall and W. M. Palmer, J. Meteor. **5**, 165 (1948). https://doi.org/10.1175/1520-0469(1948)005%3C0165:TDORWS%3E2.0.CO;2

9. M. Xie and Q. He, Particuology **70**, 64 (2022). https://doi.org/10.1016/j.partic.2022.01.006
10. J. R. Norris, Ann. Appl. Prob. **9**, 78 (1999). https://doi.org/10.1214/aoap/1029962598
11. L. M. Hocking and P. R. Jonas, Quarter. J. Royal Meteor. Soc. **96**, 722 (1970). https://doi.org/10.1002/qj.49708536305
12. K. F. Moore, D. E. Sherman, J. E. Reilly, and J. L. Collett, Atmos. Environ. **38**, 1389 (2004). https://doi.org/10.1016/j.atmosenv.2003.12.013
13. K. N. Liou and S. C. Ou, J. Geophys. Res.: Atmos. **94**, 8599 (1989). https://doi.org/10.1029/JD094iD06p08599
14. J. W. Telford, J. Atmos. Sci. **12**, 436 (1955). https://doi.org/10.1175/1520-0469(1955)012%3C0436:ANAOCT%3E2.0.CO;2
15. D. T. Gillespie, J. Atmos. Sci. **29**, 1496 (1972).
16. F. Gebauer, J. Villwock, M. Kraume, and H. J. Bart, Chem. Eng. Res. Des. **115**, 282 (2016). https://doi.org/10.1016/j.cherd.2016.09.037
17. S. I. Shima, K. Kusano, A. Kawano, T. Sugiyama, and S. Kawahara, Quarter. J. Royal Meteor. Soc. **135**, 1307 (2009). https://doi.org/10.1002/qj.441
18. P. Bartman, O. Bulwnok, K. Góeaki, A. Jaruga, G. Łazarski et al., The J. Open Source Software **7**, 3219 (2022). https://doi.org/10.21105/joss.03219
19. M. J. Bartholomew, Disdrometer and Tipping Bucket Rain Gauge Handbook (ARM Climate Research Facility, 2009). https://doi.org/10.2172/1019411
20. P. Embrechts, The Bell Curve is Wrong: So What? Extremes and Integrated Risk Management (2000). https://api.semanticscholar.org/CorpusID:161987296
21. O. Catoni, Ann. IHP Probab. Stat. **48**, 1148 (2012). https://doi.org/10.1214/11-AIHP454
22. M. Ahsanullah, B. M. Kibria, and M. Shakil, "Normal Distribution," in Normal and Student's T Distributions and Their Applications (Atlantis Press, Paris, 2014) pp. 7–50.
23. D. M. Whelpdale and R. List, J. Geophys. Res. **76**, 2836 (1971). https://doi.org/10.1029/JC076i012p02836
24. E. G. Bowen, Aust. J. Chem. **3**, 193 (1950). https://doi.org/10.1071/CH9500193
25. S. Twomey, J. Atmos. Sci. **23**, 405 (1966). https://doi.org/10.1175/1520-0469(1966)023%3C0405:CORFBC%3E2.0.CO;2